Oscillations of low-current electrical discharges between parallel-plane electrodes. I. dc discharges

Z. Lj. Petrović* and A. V. Phelps†

Joint Institute for Laboratory Astrophysics, University of Colorado and National Institute of Standards and Technology, Boulder, Colorado 80309-0440

The oscillatory behavior of dc discharges between parallel-plane electrodes (1 cm spacing) at low pressures (0.5–3 Torr) is measured and compared with models. For hydrogen these discharges are unstable for wide ranges of discharge current below 0.2 mA/cm^2 and external circuit resistances above ≈ 4000 Ω. Lateral constrictions of the discharge occur over a much more limited range of currents and pressures than do oscillations. Laser-induced photoelectron pulses produce damped oscillations for discharge currents below those at which self-sustained oscillations are observed. The frequency of the oscillations varies approximately as the square root of the discharge current and the damping of the oscillations increases with the discharge current. These results agree with simple models developed in an accompanying paper [this issue, Phelps, Petrović, and Jelenković, Phys. Rev. E **47**, 2825 (1993)]. Some data are presented for argon and nitrogen.

PACS number(s): 52.80.Dy, 52.80.Hc, 52.40.Hf

I. INTRODUCTION

Interest in the cathode regions of electrical discharges in gases has undergone a revival in recent years because of the availability of high-speed computers for use in modeling the very complex combination of physical processes occurring in these discharges [1–3] and because of the application of low-pressure discharges to plasma processing [4], switches [5], and lasers [6]. In this and the following two papers, to be referred to as papers II [7] and III [8], we extend and apply experimental diagnostics and simple models developed for investigations [9–11] of electrical discharges at very low currents and very high E/n to investigations of the optical and electrical behavior of electrical discharges at low-current densities such that space-charge effects are just becoming significant. Here E/n is the ratio of the electric field E to the gas density n. At these current densities, i.e., roughly 0.1 to 200 μA/cm^2 at H$_2$ pressures of 0.3 to 3 Torr (40 to 400 Pa), the contributions of the charged particles to the electric field are large enough to cause oscillations in the current and voltage, but are small enough so that the electric field in the discharge region is approximately uniform. dc experiments in H$_2$ at high enough currents such that the electric field is measurably perturbed are the subject of recent measurements [12,13]. In this paper we present results for dc discharges in H$_2$, N$_2$, and Ar. We emphasize H$_2$ discharges because the H$_2$ metastable lifetimes are very short at the pressures of interest [14] and because moderate current H$_2$ discharges can be used to produce reasonably stable electrode surfaces [15].

The motivation for this series of investigations grew, in part out of the observation that published data [16] for dc discharges dominated by the cathode fall show a very wide range of operating voltages, particularly at low pressures and low currents. Although Penning and co-workers [1,17] have shown that one can obtain reproducible results by proper electrode preparation and gas purification techniques, one does not know how to predict the voltage-current characteristic of discharges with practical electrodes from auxiliary measurements. The present work is one of many investigations currently being undertaken [2,3,13] to develop the understanding necessary for modeling such discharges.

There have been relatively few publications concerned with oscillations in low-current, low-pressure, parallel-plane discharges [12,18–21]. Much of the experimental [20–27] and theoretical [28–30] work with parallel-plane geometry has been directed toward the determination of the equivalent circuit parameters for dc discharges with well-developed cathode-fall regions. Sigmond [18] has discussed the necessary and sufficient conditions for self-sustained or undamped oscillations at low currents and has shown that some of the work on the negative differential resistance of hydrogen discharges [19] is suspect because of a failure to test for oscillations. Gottscho and co-workers [2,20] used a laser-produced photoelectric pulse and observed damped oscillations on time scales short compared to those of our experiments. Debontride et al. [21] used very large laser-produced photoelectric pulses and do not report oscillations on their short-time scale. Our work is concerned with smaller current pulses and with the oscillations that occur on a time scale that is long compared to ion transient times. The scarcity of papers in this area is to be contrasted to the large numbers of papers concerned with oscillations and other instabilities in the positive column [31] and in high-pressure electron-beam sustained laser discharges [32].

A semiquantitative picture of voltage and current oscillations in low-current, parallel-plane discharges has been developed in the references cited above [1,18,19,22–30]. One feature is that the electron-avalanche and ion-feedback processes result in time lags in the buildup of current relative to the applied voltage. Thus, the discharge acts like an inductor, while the electrodes and circuit wiring form a capacitance. A second feature is

the frequently measured but not quantitatively understood negative differential resistance of these discharges. At lower currents the inductance of the discharge is large and the impedance of the system is that of a damped oscillator. At higher currents the inductive component of the discharge decreases and together with the negative resistance causes the damping to become negative, i.e., one observes the onset of oscillations that grow in amplitude and become very nonsinusoidal. Thus far, quantitative comparisons of experiment with theory [18] have been limited to tests of the conditions for the onset of nonlinear oscillations with calculations based on the inductance and negative resistance measured at low currents.

The primary contribution of this series of papers is to present in papers I and II considerably more extensive and accurate measurements of the dc and oscillatory properties of such discharges in H_2 under conditions of reproducible, although poorly understood, cathode conditions. Secondarily, we present in paper III a simple model based on the measured negative differential resistance that explains quantitatively the oscillatory behavior and a second model that predicts the approximate magnitude of the discharge negative differential resistance. While these almost analytic models will no doubt be supplanted by more accurate and detailed models, the experimental data are essential for testing all models and are presented first. The more theoretically inclined reader may wish to begin with paper III.

The paper is concerned with the systematic measurement of (i) voltage-current characteristics of discharges in H_2, N_2, and Ar over a wide range of currents, (ii) the discharge and external circuit conditions that result in spontaneous oscillations and constrictions in low-current dc discharges, and (iii) the frequencies and damping constants of transient oscillations produced by laser-induced photoelectron pulses. The results will be used to test the applicability of the model developed in paper III of this series. Data obtained using a pulsed voltage technique for low-current discharges are presented in paper II. The experimental apparatus is described in Sec. II. Measurements of voltage-current characteristics are summarized in Sec. III. Sections IV and V describe the determination of the conditions for which the discharge in H_2 is unstable and for which the discharge is constricted. Measurements of the laser-induced transient oscillations are presented in Sec. VI. Experiment and theory are compared in Sec. VII.

II. EXPERIMENTAL TECHNIQUE

Figure 1 shows a schematic of the discharge tube developed for these measurements of the properties of low-pressure, parallel-plane discharges. The cathode C is made of gold-plated copper and is operated at a high voltage relative to the grounded vacuum shell. A thermocouple in contact with the copper cathode measures the cathode temperature. The gold provides a relatively stable work function, while the copper base has the thermal capacity to keep the temperature rise small and the thermal conductivity to keep the gold surface and the
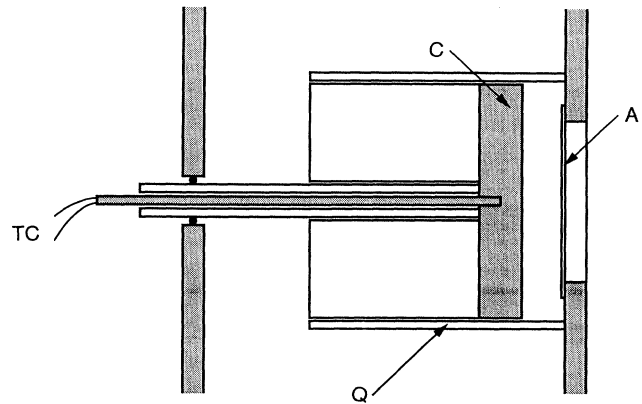

FIG. 1. Schematic of discharge tube. Here C is the cathode, A is the anode, Q is the quartz cylinder, and TC is a thermocouple for measuring the rise in cathode temperature.

thermocouple at the same temperature. The electrode spacing d is adjustable, but is 1.05 cm for the present experiments. The thermocouple TC and its meter operate at the high voltage of the cathode, but are disconnected during measurements of oscillation characteristics so as to reduce the circuit capacitance. The cathode lead is covered with glass and the cathode is surrounded with a tightly fitting quartz cylinder Q that prevents long-path breakdown at low pressures [1,9]. The anode A is a semi-transparent film of gold or AuPd [15] deposited on a quartz window so as to allow observation of lateral constrictions of the discharge. The semitransparent area is 6 cm in diameter and is insulated from the ground for current measurements.

A schematic of the electrical circuit is shown in Fig. 2. All of the data reported in this paper are obtained with a simple electrical circuit consisting of resistance R_S connected to the cathode in series with the discharge D and a
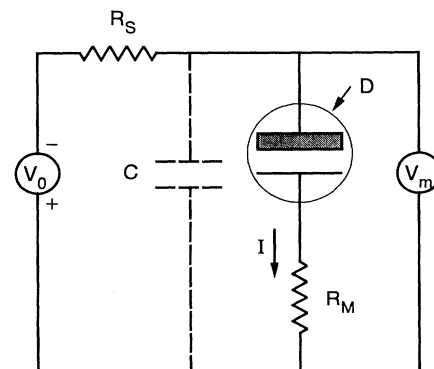

FIG. 2. Schematic of electrical circuit. Here D is the discharge tube, R_S is the series or current limiting resistor, R_m is the resistor for monitoring the discharge current I, C is the capacitance of the discharge tube leads and electrodes, and V_0 and V_m are the power supply voltage and total measured voltage.

current-monitor resistor R_m between the anode and the ground. Both resistors are external to the discharge and the capacitance C due to the cable and lead capacitance exceeds the capacitance of the discharge electrodes by a factor of 6 [33]. The series resistor R_S is increased from 1 kΩ to 200 MΩ as the average current is decreased. The monitor resistor R_m is varied from 50 Ω to 10 kΩ so as to provide suitable voltages for an analog-to-digital converter. The voltage V_0 is supplied from a dc, voltage-regulated supply. In some of the experiments the stability characteristics of the discharge were modified by changing the capacitance C shunting the discharge [33].

The average discharge currents I are measured with a dc electrometer and transferred to a digitizer and personal computer for storage and analyses. Similarly, the voltage V_m across the discharge tube is measured with a high-impedance (100 MΩ) voltage divider and dc electrometer and then digitized and stored in the computer. Gas pressures p are measured with a diaphragm-type manometer with a stated accuracy of ±0.01 Torr, where 1 Torr = 133 Pa. The gas samples are taken from high-pressure cylinders with a stated purity of 0.9999. The rate of rise of pressure after overnight evacuation and mild baking is $\approx 5 \times 10^{-4}$ Torr/h.

Current oscillations are detected with a wide-band oscilloscope, but under some conditions the effective response time is limited by cable capacitance and varies from about 10 μs for $R_m = 10$ kΩ to about 100 ns for $R_m = 100$ Ω. The discharge is designated as oscillating when the peak-to-peak amplitude reached 10% of the average current. Small amplitude ($\approx 5\%$), randomly timed, highly damped, high-frequency (≈ 1 MHz) oscillations observed at low currents ($< 10^{-5}$ A) with H_2 at 0.5 Torr are not designated as oscillations in this paper. The transient current and voltage wave forms were recorded with the storage oscilloscope and then transferred to the computer. For the data shown, 4 to 64 sweeps were made at a 10-Hz repetition rate.

For the transient measurements, the cathode is illuminated through the semitransparent film with the quadrupled output (266 nm) of a neodymium-doped yttrium aluminum garnet (Nd:YAG) laser [34]. The average cathode currents were < 2 nA, corresponding to < 0.2 nC per 10 ns for a 20-mJ laser pulse at a repetition rate of 10 Hz. The electric-field distortion introduced by the space charge resulting from these pulses and the subsequent discharge avalanche is small, but not negligible. Considerable downward drift of the photocurrent occurs during the experiment because of decreases in the laser output and in the photocathode yield. Since most of the measurements reported here are in the small perturbation range, the discharge response was proportional to the photoelectron pulse and the primary effect of the changing photoemission was a loss of signal amplitude. As discussed in Sec. VII, a drift in the dc current is more serious. In the case of nitrogen discharges the decrease in photoelectric yield resulted in the disappearance of signal in a few minutes and prevented transient measurements using this technique. It is to be noted that the cathode emission recovered from the nitrogen discharge after pumping the system overnight. This behavior suggests

that the cathode was poisoned by driving nitrogen ions or neutral species onto or only a short distance into the gold cathode and that the nitrogen atoms leave the gold after a few hours exposure to vacuum.

Initially, considerable difficulty was encountered in obtaining reproducible dc discharge operating voltages. Especially at low pressures, the discharge voltage at currents below about 1 μA was found to drift badly as the discharge was operated. An aging procedure was adopted that resulted in reproducible voltages, i.e., the discharge was operated for ≈ 10 min at a current of 0.5 mA and a pressure of 1 Torr of H_2. The aging current was chosen to give a laterally uniform discharge, i.e., no visible constriction. In addition, an increase in the low-current operating voltage was observed following discharge operation at high currents. This effect is attributed to a reduction in the gas density and, thereby, a reduction in the ionization rates resulting from changes in the cathode and gas temperature, i.e., ≈ 10 K for 30 mA for 10 s. The return to the low-current operating voltage was observed to correspond to the recovery time constant of 5–10 min for the cathode temperature as observed with the thermocouple. For this reason, an effort was made to minimize the time required for voltage-current measurements at the higher currents.

An additional problem encountered was the sputtering of gold from the cathode onto the semitransparent anode and onto the quartz side walls. See paper II for a solution to the cathode heating problem and a partial solution to the sputtering problem using pulsed voltages.

The choice of pressures used in these experiments was based in part on the desire to cover the same pressure range to be used in measurements of the properties of discharges dominated by the cathode fall at higher currents than used in the present work. Because of our limited spatial resolution for optical emission measurements and limited maximum electrode separation, this meant that the pd values were chosen to be between 0.5 and 3 Torr cm, so that with 1.05-cm electrode separation the pressures were limited to between 0.5 and 3 Torr.

III. VOLTAGE-CURRENT MEASUREMENTS

Representative measurements of the average discharge voltage as a function of the average current density in H_2 are shown in Fig. 3 for pressures of 0.5 and 1 Torr. The abscissa is labeled as the *average* current density because nonuniformities in discharge brightness and, presumably, current density occur across the cathode surface for current densities of the order of 10^{-4} A/cm². Current densities are shown because we expect the data, including the region of oscillations, to scale with current density [1,9]. We have not investigated this scaling. The data of Fig. 3 show that for current densities below about 10^{-5} A/cm² the discharge operating or maintenance voltage is independent of current at low currents. This low-current limit of the discharge maintenance voltage is equal to the minimum breakdown voltage in the limit of zero current [1]. We will refer to this limiting voltage as the breakdown voltage V_B in this and the accompanying papers
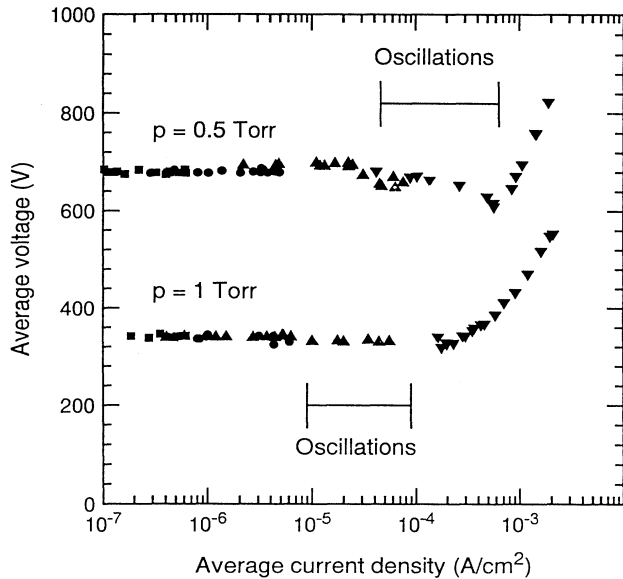
FIG. 3. Average voltage vs average current density for H_2 discharge at $pd = 0.525$ and 1.05 Torr cm. The series resistances and symbols used are 8.8 MΩ, ■; 1 MΩ, ●; 50 kΩ, ▲; 1 kΩ, ▼.

[7,8]. We will see that it serves as a run-to-run measure of the cathode condition.

For average currents in the 10^{-5} to 10^{-3} A/cm^2 region we observe the various temporal instabilities, including oscillations about the average current, that are the subject of these papers. There is also a rather large scatter in the voltages for current densities in the 3×10^{-5} to 10^{-3} A/cm^2 range for the 0.5 Torr data shown in Fig. 3. This scatter is the result of instabilities, such as temporal oscillations and discharge-voltage discontinuities or hysteresis effects in the discharge-voltage–current characteristic.

At the highest currents shown the discharges are electrically stable, but are subject to gas heating and rapid electrode modification. Similar data were obtained at 3 Torr and breakdown voltages of about 400 V. In order to obtain data over a wide range of currents, the series resistance is varied from 1 kΩ to 200 MΩ. The current range covered with each resistor is roughly a factor of 10, e.g., 10^{-6} to 3×10^{-5} A with a series resistor of 9 MΩ. The data shown at high-current densities are obtained in a few seconds so as to minimize changes in the cathode surface and gas temperature and the resultant changes in the low-current operating voltage.

Oscillations and discharge constrictions will be discussed in Secs. IV and V and models of the oscillations from paper III will be compared with experiment in Sec. VII. Similar results are obtained for discharge current densities of the order of 10^{-4} and 10^{-5} A/cm^2 for pressures of 1 and 3 Torr.

The voltage-current data in Fig. 3 are similar in form but different in magnitude from those obtained previously by Güntherschulze [35] and by Klyarfel'd, Guseva, and Pokrovskaya-Soboleva [36]. The large variation in V_B

voltage with experiment is attributed primarily to differences in cathode conditions. See Sec. III E of paper III.

IV. STABILITY CHARACTERISTICS

Figures 4 and 5 show the "stability limits" for the H_2 discharges at pressures of 0.5 and 3 Torr. In these figures we have plotted the current rather than the current density versus the series resistance R_S, since some of the limits to be shown on such a plot in paper III do not scale with current density. Two types of instability are indicated in these figures, i.e., oscillations and jumps. Here the discharges are defined as oscillatory when the amplitude of self-sustained current oscillations exceeds 10% of the average current. The measured limits of oscillation are indicated by the points and a solid curve has been drawn through the points. Thus, the discharges exhibit self-sustained oscillations inside the region outlined by the solid curve. The temporal variations of the self-sustained current oscillations are discussed at the end of this section. The experimentally determined limits to self-sustained oscillations shown in Fig. 5 are compared with theory in Sec. VII. The quantitative correlation of regions of oscillation with the series resistance shown in Figs. 4 and 5 does not appear to have been noted in previous publications [1].

The second type of instability shown in Figs. 4 and 5 is that in which the use of a series resistance R_S that is too
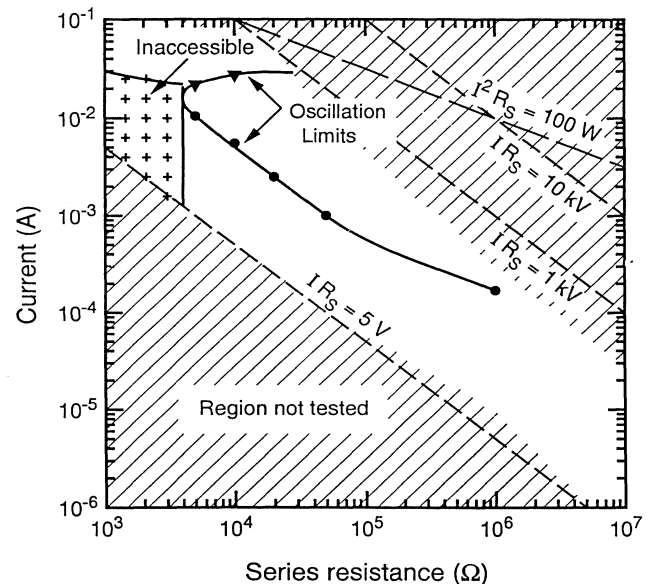

FIG. 4. Stability diagram for H_2 discharge for $pd = 0.525$ Torr cm, $R_m = 100$ Ω, $C = 250$ pF, and an electrode area of 50 cm^2 plotted on the average discharge current I and series resistance R_S plane. The solid circles and triangles are experimental lower and upper limits for self-sustained oscillations and are connected by a smooth curve for identification only. The shaded regions are not examined. Points within the region marked "inaccessible" cannot be reached with our circuitry.
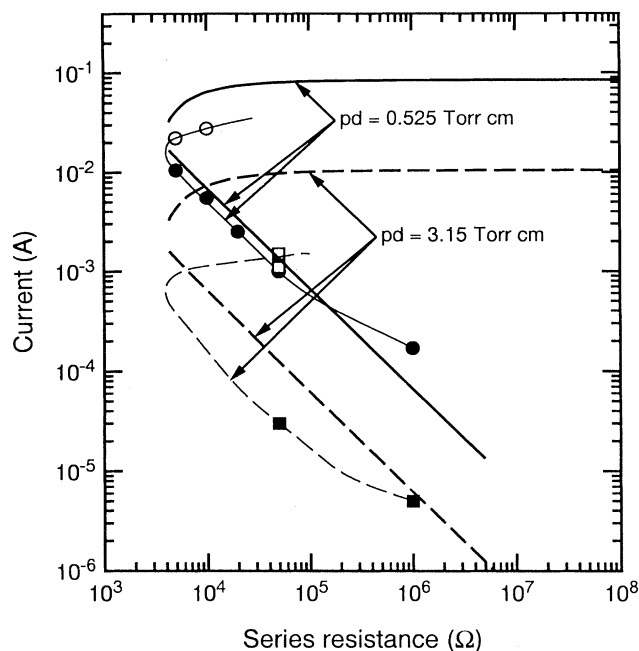
FIG. 5. Stability diagrams for H_2 discharges at $pd = 0.525$ (solid curves) and 3.15 Torr cm (dashed curves), $R_m = 100 \ \Omega$, and $C = 250$ pF. Data for 1.05 Torr cm have been omitted for clarity. The light curves serve to connect experimental data, while the heavy curves are predictions of the model for $R_m = 100 \ \Omega$ and $R_D = -4000 \ \Omega$.

small results in a jump of the current to high currents, e.g., ≈ 10 mA, when the discharge voltage is increased above breakdown. For discharges in H_2 at 0.5 Torr, Fig. 4 shows that this effect results in a region that is "inaccessible." This instability is very well known in the literature [1,18,22–30] and is ascribed to the negative slope of the voltage-current characteristic of electrical discharges. The negative differential resistance behavior is modeled in Sec. IV of paper III in terms of changes in ion-induced electron yields at the cathode resulting from space-charge distortion of the discharge electric field.

The shaded portions of Fig. 4 show regions of current and resistance not investigated for a discharge pressure of 0.5 Torr. Similar regions were not investigated at the other pressures. The upper limits to the shaded region shown in the lower left corner of Fig. 4 were determined by our inability to maintain the power supply voltage within about 5 V of the drifting discharge operating voltage. The lower limits to the shaded region shown in the upper right corner of Fig. 4 were set by the voltages available from the power supplies and/or by the power dissipation allowable in the series resistors. The dashed lines in Fig. 4 show the calculated voltage drops across the series resistor IR_S and the power dissipation I^2R_S in the series resistor.

The data of Fig. 4 show that by a proper choice of R_S and power supply voltage we can, in principle, operate a discharge at $p = 0.5$ Torr and $d = 1$ cm without self-sustained oscillations at any desired current below about 2×10^{-4} A/cm^2 and above 1.2×10^{-4} A/cm^2 using the

circuit of Fig. 2. A similarly large range of currents can be covered at 1 Torr. For $p = 3$ Torr the drift in discharge voltage caused by changes in the cathode leads to difficulties in obtaining a stable discharge, particularly at currents near 1 μA.

The effect of changing the circuit capacitance can be measured by removing extraneous circuit elements, e.g., the thermocouple voltmeter, or by adding known capacitances in parallel with the discharge at fixed series resistance. In general, adding capacitance expanded the region of instability to lower currents. Thus, for H_2 discharges at 0.5 Torr and a series resistance of 50 kΩ, decreasing the measured circuit capacitance from 500 pF to the minimum of 250 pF set by the discharge tube construction raises the low-current limit for oscillations from 1.5 to 2.3 mA. When the circuit capacitance was increased to 0.01 μF the lower limit for oscillations decreased to 0.11 mA. The upper limit for oscillations was unchanged to within the uncertainty of the measurements.

For N_2 discharges, oscillations were observed at 3 Torr with series resistances of 1 MΩ for currents between 0.22 and 0.27 mA and with 5.5 MΩ for currents between 0.26 and 0.55 mA. No oscillations were observed for pressures of 0.5 and 1 Torr. For Ar discharges, oscillations were observed at 0.3 Torr with a series resistance of 1 MΩ for currents between 0.1 and 0.5 mA. No oscillations were observed for Ar pressures of 1 and 2 Torr. See *Note added in proof.*

Another point of interest is that the lower limits to the region of oscillations scale as the square of the pressure, i.e., the solid points in Fig. 5 nearly coincide when plotted as jp^2 versus R_S at small R_m. We can use this observation and the conventional scaling parameters [1,8] of jd^2 and pd (actually jd^2 and nd) to predict the variation in the lower limit for oscillations with electrode separation d. The combination of scaling parameters consistent with the observed pressure dependence is $jd^2(pd)^2 = jp^2d^4$, so that at constant pressure the current density for the onset of oscillations should decrease inversely as the fourth power of the electrode separation. The upper limit to the current for oscillations varies approximately as the three-halves power of pressure and so should vary as the cube of the electrode separation.

A few records are available from our experiments of the time dependences of the self-sustained current and voltage oscillations. Figure 6 shows examples of such data for a pressure of 0.5 Torr, $R_S = 50$ kΩ, $V_D = 640$ V, and $R_m = 100 \ \Omega$. The upper voltage and current wave forms are for an average current of 2.5 mA, while the lower voltage and current wave forms are for an average current of 30 mA. These and other data show a change from sharp current spikes increasing in frequency with current near the threshold current of about 2 mA. Approximately triangular current wave forms with a frequency independent of current are observed at near the high-current limit for self-sustained oscillations of 32 mA. Similar self-sustained oscillation wave forms were obtained at 1 Torr, except that just below the upper limit for oscillations the current and voltage were very nearly sinusoidal. The changes in wave forms were often ac-
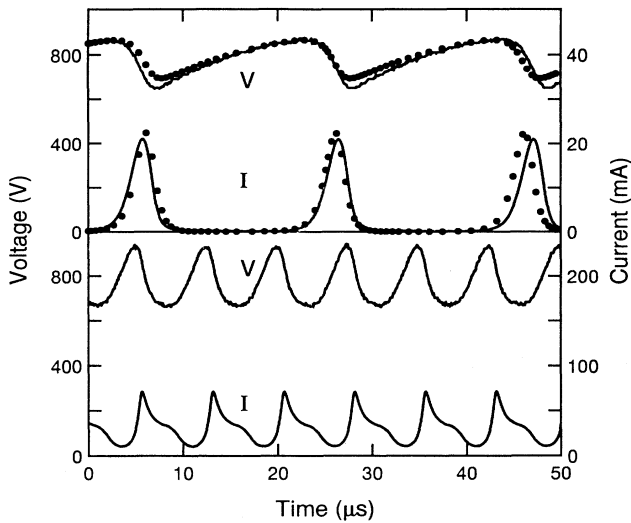
FIG. 6. Self-sustained oscillations for H_2 discharge at $pd = 0.525$ Torr cm, $R_S = 50$ kΩ, and $R_m = 100$ Ω. The upper voltage V and current I curves were obtained for an average current of 2.5 mA compared to current at the onset of oscillations of 2 mA. The lower voltage V and current I curves were obtained for an average current of 30 mA compared to the maximum for self-sustained oscillations of 32 mA. The dots shown in the upper traces were calculated using Eqs. (9) and (10) of paper III, using coefficients described in the Appendix of paper III.

companied by discontinuous changes in average discharge voltage. The wave forms of Fig. 6 are consistent with the numerous studies of "relaxation" oscillations often made in commercial discharge tubes with more complex electrode geometries [37]. It should be noted that although operation of the discharge with $R_m = 10$ kΩ results in the absence of large self-sustained oscillations for the currents used in our experiments, there are very small-amplitude, high-frequency oscillations that were not investigated systematically.

The dots shown with the upper trace of Fig. 6 are the theoretical voltage and current wave form calculated using Eqs. (10) and (11) of paper III. The ion transit time, negative resistance, and ion-induced electron emission coefficient used in this calculation were obtained as described in paper III.

V. DISCHARGE CONSTRICTIONS

Observations of emission from the negative glow of low-pressure, low-current density discharges often show a significant spatial variation over the area of the discharge [1]. We will designate a discharge with such nonuniformities as a *constricted* negative-glow and/or cathode-fall discharge. These discharges are conventionally [1] given the uninformative name of a "subnormal" discharge. The case of uniform emission over the cathode surface, which is conventionally referred to as an "abnormal" glow [1], will be called the *high-current-diffuse* negative glow and/or cathode fall. No attempt is made in this pa-

per to show the transition between constricted and diffuse negative-glow discharges in the form of Figs. 4 and 5. No bright localized regions are seen in H_2 at pressures of 0.5 and 1 Torr and currents from 10^{-6} to 10^{-1} A even though steps (too small to be seen in Fig. 3) are observed in the voltage as the current is increased to near and above the onset of oscillations. These steps correlate with changes in the time-dependent voltage wave form. At a pressure of 3 Torr of H_2 "constrictions," i.e., doughnut-shaped brighter regions near the quartz cylinder that increased in area as the current increased, were observed at currents between 1.5 and 10 mA. Constrictions are not detected at currents above the threshold for visual observation at about 10 μA and below the onset of oscillations. No "hot spots" are observed near the wall in the vicinity of the anode [12].

Constrictions are observed with Ar discharges for pressures of 1 and 2 Torr and currents from 3×10^{-5} to 3×10^{-3} A. For 0.3 Torr of Ar, constrictions are observed for currents from 1.5×10^{-4} to 10^{-3} A. For N_2 discharges constrictions are observed for currents between 0.3 and 2 mA at 0.3 Torr, between 0.05 and 3 mA at 1 Torr, and 0.1 and 30 mA at 3 Torr. At 0.3 Torr the brightness of the constricted area increases as the current increases, rather than the usual [1] fixed brightness and increasing area.

VI. LASER-INDUCED DISCHARGE OSCILLATIONS

Figures 7 and 8 show representative wave forms resulting from a laser-induced photoelectron pulse emitted from the cathode of low-current, low-pressure discharges in hydrogen. Figure 7 illustrates the variation in current
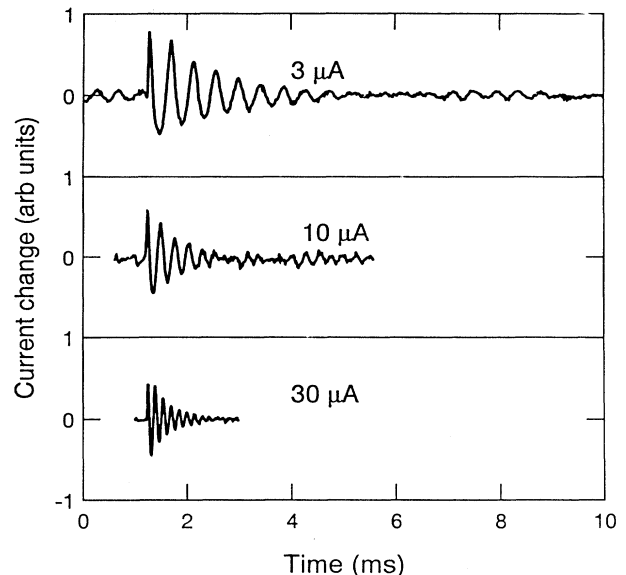

FIG. 7. Photoelectron-induced transient current wave forms in H_2 for a $pd = 0.525$ Torr cm, $R_S = 5$ MΩ, and $R_m = 10$ kΩ showing the variation of frequency and damping with dc discharge current.
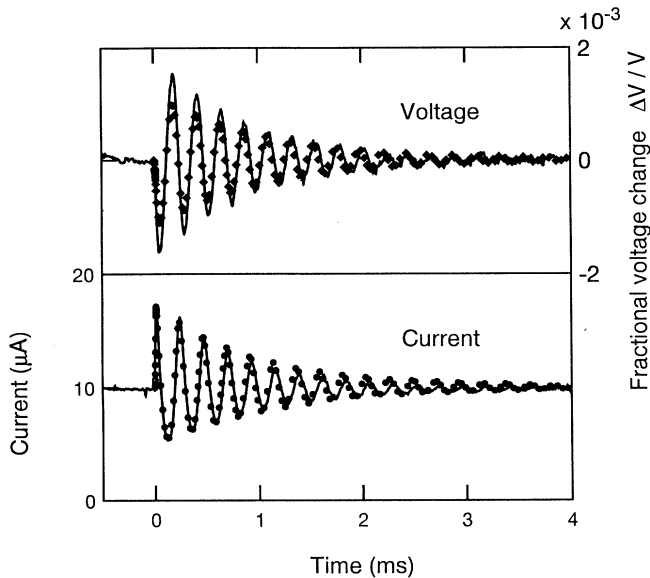
FIG. 8. Photoelectron-induced transient current and voltage wave forms in H_2 for a $pd = 0.525$ Torr cm, $R_S = 5$ MΩ, and $R_m = 10$ kΩ. The solid curves are from experiment and the points are the results of calculations using the model of paper III.

FIG. 9. Angular frequency ω and damping constant κ vs current for $pd = 0.525$ Torr cm. The points are measurements for $R_m = 10$ kΩ and $R_S = 5$ MΩ. The solid and dashed curves are calculated using Eq. (2) for $R_m = 10$ KΩ and 100 Ω, respectively, and $R_S = 5$ MΩ.

wave form with dc discharge current, while Fig. 8 compares the observed and calculated current and voltage change wave forms. The duration of the photoelectron current pulses is $\approx 10^{-8}$ s. The data shown is for a pressure of 0.5 Torr, $R_S = 5$ MΩ, and $R_m = 10$ kΩ. While the changes in discharge current can be large, the voltage oscillations are only a small fraction of the discharge voltage. As discussed in paper III, the currents were small enough so that the calculated space-charge distortion of the electric field was small but not negligible. The applied E/n values ranged from E/n for which the electrons are in equilibrium with the gas, i.e., ≈ 300 Td at 3 Torr, to E/n where nonequilibrium effects are important, i.e., 4 kTd at 0.5 Torr. The frequencies ranged from 2 to 30 kHz and the damping time constants were from 100 μs to 1 ms. When using the photoelectric technique for producing the initial current pulses, many transients are required to obtain a good signal to noise. The upper limit of the dc discharge current for these observations was determined by the onset of continuous oscillations shown in Figs. 4 and 5 and discussed in Sec. IV. The lower limit to the current used was set by an overdamped transient as the current and voltage approach steady state. These transient experiments complement the earlier ac impedance measurements for steady-state hydrogen discharges, e.g., the measurements of Sigmond [18] at higher pressures and a lower electrode separation. The comparison of the model of paper III and experiment in Fig. 8 is discussed in Sec. VII.

Measured angular frequencies ω and damping constants κ, i.e., the reciprocal of the damping time constant, are shown in Fig. 9 as a function of the discharge current for a hydrogen pressure of 0.5 Torr. A model for these
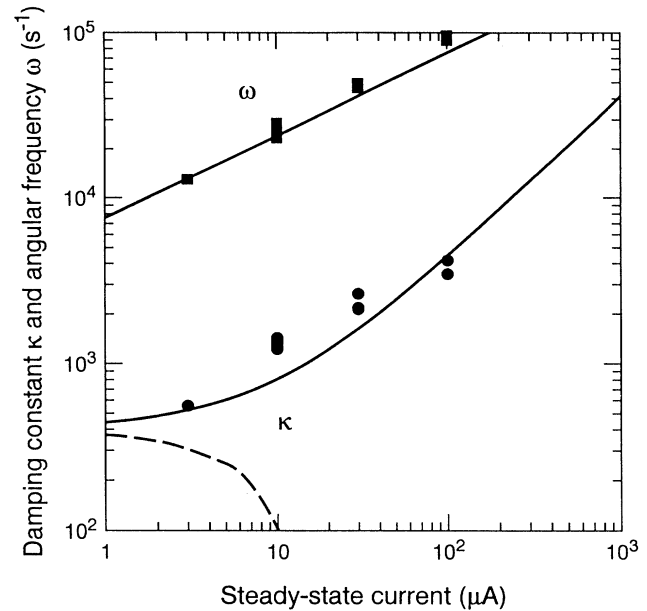
experiments is derived in paper III and the experimental results are compared with the model in Sec. VII.

VII. COMPARISON OF MODEL AND EXPERIMENT

The model derived in paper III is based on the following assumptions: the avalanche regeneration time is determined by a fixed ion transit time that is short compared to the times of interest; the ionization is produced only by electrons and is given by a local electric-field model; electrons are produced at the cathode only by ions and fast atoms; and space-charge distortion of the electric field is small but not negligible. These assumptions, along with the circuit shown in Fig. 2, lead to two coupled nonlinear differential equations describing the transient discharge voltage and current.

Figure 8 shows a comparison of the theory and experimental current and voltage wave forms for $p = 0.5$ Torr, $R_S = 5$ MΩ, $R_m = 10$ kΩ, and a steady-state discharge current of 10 μA. The solid lines denote experimental data and the points are the results of a calculation carried out with the full nonlinear equations given in Eqs. (10) and (11) of III. As discussed in paper III, most of the parameters are determined from other experiments so that the only fitting parameter for Fig. 8 is the magnitude of the charge transferred across the discharge gap by the photoelectrons. Thus, the discharge parameters used in this calculation are based on a fit to the measured angular frequencies for an average of the data of papers I and II and result in an ω that is only $\approx 1\%$ too small for the op-

timum fit in Fig. 8.

The initial increase in discharge current ΔI in Fig. 8 is found by solving Eq. (10) of III for a laser-induced photocurrent of amplitude I_P. For a laser pulse of duration Δt that is short compared to the time characteristic of current growth and voltage change, the result is

$$\Delta I = (1+\gamma)(I_p \Delta t)/(\gamma T) , \tag{1}$$

where γ is the yield of electrons per ion arriving at the cathode and T is the effective ion transit time. The peak current ΔI at the end of the initiating pulse is that caused by the ions produced by the photoelectrons and is determined by the charge $I_p \Delta t$ transferred during the pulse, the number of ions produced per electron leaving the cathode $1/\gamma$, and the ion transit time T. The fit shown was obtained with a laser-induced photoelectron peak current 10^{-8} A and a pulse of 10 μs duration for a photoelectron charge transferred during this simulation pulse of $I_p \Delta t = 10^{-13}$ C. The pulse length was chosen for computational convenience and in order to simulate the ≈ 10 μs response time of the current transient recording system when using $R_m = 10$ kΩ. The small charge transfer per pulse is necessary to fit the observed amplitude, but is surprising since we usually observed much larger charge-transfer values of 10^{-10} C/pulse corresponding to average vacuum currents of 1 nA.

The upper solid curve of Fig. 9 shows the predicted variation of the angular frequency ω of the damped oscillations with current. According to Eq. (20) of III, ω is given by

$$\omega^2 = \frac{I_{SS}}{R_S CT} \left[(R_S + R_m)\frac{\partial g}{\partial V} - \frac{k_I}{\gamma_{SS}} \right]$$

$$\times \left[1 + \frac{I_{SS}(k_I - R_m k_V)}{\gamma_{SS}(1+\gamma_{SS})} \right]^{-1} - \kappa^2 , \tag{2}$$

where k_V and k_I are defined by the expression for the ion-induced electron emission coefficient γ as

$$\gamma = \gamma_p + k_V V + k_I I , \tag{3}$$

γ_p is the electron yield at zero V and I, I_{SS} and γ_{SS} are the steady-state discharge current and electron yield, $\partial g/\partial V$ is the change in electron number gain with voltage, and κ is the damping constant. The electron number gain g is the ratio of electron flux produced by ion-induced electron emission to the flux of electrons leaving the cathode and in our model [8] is unity as required for a steady-state discharge. For $\omega^2 \gg \kappa^2$, Eq. (2) can be written as

$$\omega^2 = \frac{1}{LC} \left[1 + \frac{(R_m + R_D)}{R_S} \right] , \tag{4}$$

where the equivalent circuit inductance and resistance are discussed in III and are defined by $L = T/(I_{SS}\partial g/\partial V)$, and $R_D = -k_I/(\gamma_{SS}\partial g/\partial V)$. This model is consistent with the discharge model in terms of lumped-circuit elements discussed by Sigmond [18]. The upper solid line of Fig. 9 is calculated using Eq. (2) and is

the same for R_m values of 10 kΩ and 100 Ω. The series resistance is 5 MΩ. The ion transit time deduced from the angular frequency using Eqs. (2) or (4) and calculated values of g is 80 ns. This value is longer than the 40-ns free-fall transit time for H$^+$ for 1.05 cm, but comparable with the ≈ 100 ns obtained by extrapolating our measurements [38] of the time of maximum ion current in H$_2$ to a 1.05-cm drift distance and $E/n \approx 4$ kTd. Here 1 Td (townsend) $= 10^{-21}$ V m^2. Questions of the use of angular frequency measurements for ion transit time determination, ion identification, etc. are discussed further in III.

The lower curves of Fig. 9 show the predicted damping coefficients κ as derived in III and given by

$$\kappa = \frac{1}{2R_S C} \left[1 + \frac{I_{SS}[k_I - (R_S + R_m)k_V]}{\gamma_{SS}(1+\gamma_{SS})} \right.$$

$$\left. - \frac{R_S C I_{SS}}{T} \left[\frac{k_I}{\gamma_{SS}} - R_m \frac{\partial g}{\partial V} \right] \right]$$

$$\times \left[1 + \frac{I_{SS}(k_I - R_m k_V)}{\gamma_{SS}(1+\gamma_{SS})} \right]^{-1} . \tag{5}$$

In the limit of low currents I_{SS} this can be written as

$$\kappa = \frac{1}{2R_S C} + \frac{[R_m - (-R_D)]}{2L} . \tag{6}$$

The solid and dashed lines are calculated for R_m values of 10 kΩ and 100 Ω, respectively, while the series resistance is 5 MΩ in both cases. In contrast to the situation for the angular frequency, we see that the damping is a strong function of R_m. Thus, the use of a large current-monitor resistor, i.e., 10 kΩ, in the experiments shown in Figs. 7, 8, and 9 prevented the appearance of self-sustained oscillations. With a small monitor resistor, e.g., $R_m = 100$ Ω and $R_S = 5$ MΩ, Eq. (6) predicts damped oscillations for steady-state currents of less than about 150 μA and self-sustained oscillations for higher currents. As in earlier studies [1,18,22,25–29], Eq. (6) shows that when $R_m = 0$ self-sustained oscillations occur when the series resistor is greater than the value given by $R_S^{tr} = L/(-R_D C)$.

The experimental damping coefficients shown in Fig. 9 are equal to or larger than the theoretical values. One possible explanation of the larger experimental values is that during the 3 to 6 s duration of the measurement there are changes in the frequency of the damped oscillations caused by changes in discharge current. The changes in frequency could result in cancellation between late-time oscillation cycles recorded at different times and so produce an apparent excess damping. If this effect is occurring one might observe beats in the recorded wave form, such as seen in the data of Fig. 7. Note, however, that these apparent beats could also be transients initiated by noise pulses.

Finally, we note that the results of the model calculations from Sec. III C of paper III shown in Fig. 5 agree with the general behavior of the oscillation limits, but there are significant differences. In particular, the calculated lower limits to the undamped oscillations vary less

rapidly with pressure than do the experimental limits. This discrepancy probably is associated with the transition from ion-induced electron emission to photon-induced electron emission at the cathode [1,7,8,19]. The upper limits for undamped oscillations predicted by the low-current models of paper III are not expected to be quantitatively correct at the high-current densities of the observed limits because of severe space-charge distortion of the electric field.

VIII. SUMMARY

The experiments with low-current (<2 mA/cm^2), low-pressure (0.5 to 3 Torr) hydrogen discharges described in this paper yield the dependences on external resistance of the lower and upper limits to the current for which self-sustained oscillations occur. The region of oscillations expands to lower currents as the discharge pressure and circuit capacitance are increased. Lateral constrictions of the discharge occur over a much more limited range of currents and pressures than do oscillations. Laser-induced photoelectron pulses produce damped oscillations for discharge currents below those at which

self-sustained oscillations are observed. The frequency and damping of these oscillations increase with discharge current in approximate agreement with models developed in an accompanying paper [8]. Similar experimental results are obtained for argon and nitrogen.

Note added in proof. We have recently found a reference to experiments with Ne that is similar to those described in Secs. III and IV for H$_2$. See V. N. Melekhin and N. Yu. Naumov, Zh. Tekh. Fiz. **54**, 1521 (1984) [Sov. Phys. Tech. Phys. **29**, 888 (1984)].

ACKNOWLEDGMENTS

*Permanent address: Institute of Physics, P.O. Box 68, 11080 Zemun, Yugoslavia.

†Also with the Physics Department, University of Colorado, Boulder, CO 80309-0390.

[1] M. J. Druyvesteyn and F. M. Penning, Rev. Mod. Phys. **12**, 87 (1940); G. Francis, Handb. Phys. **22**, 53 (1956).

[2] See, for example, the experiments described by E. A. Den Hartog, D. A. Doughty, and J. E. Lawler, Phys. Rev. A **38**, 2471 (1988); A. Mitchell, G. R. Scheller, R. A. Gottscho, and D. B. Graves, *ibid.* **40**, 5199 (1989).

[3] See, for example, the models described by J.-P. Boeuf, in *Physics and Applications of Pseudosparks,* edited by M. A. Gundersen and G. Shaefer (Plenum, New York, 1990), p. 255; T. J. Sommerer, W. N. G. Hitchon, and J. E. Lawler, Phys. Rev. A **39**, 6356 (1989).

[4] See, for example, J. W. Butterbaugh, L. D. Baston, and H. H. Sawin, J. Vac. Sci. Technol. A **8**, 916 (1990); M. A. Lieberman and S. E. Savas, *ibid.* **8**, 1632 (1990).

[5] See, for example, J. Christiansen, in *Physics and Applications of Pseudosparks* (Ref. [3]), p. 1. See also other papers in this volume.

[6] B. E. Cherrington, *Gaseous Electronics and Gas Lasers* (Pergamon, Oxford, 1979), Chaps. 10–12.

[7] B. M. Jelenković, K. Rózsa, and A. V. Phelps, Phys. Rev. E **47**, 2816 (1993), referred to as paper II.

[8] A. V. Phelps, Z. Lj. Petrović, and B. M. Jelenković, this issue, Phys. Rev. E **47**, 2825 (1993), referred to as paper III.

[9] B. M. Jelenković and A. V. Phelps, Phys. Rev. A **36**, 5310 (1987).

[10] A. V. Phelps and B. M. Jelenković, Phys. Rev. A **38**, 2975 (1988).

[11] Z. Lj. Petrović, B. M. Jelenković, and A. V. Phelps, Phys. Rev. Lett. **68**, 325 (1992).

[12] B. N. Ganguly and A. Garscadden, J. Appl. Phys. **70**, 621 (1991).

[13] B. M. Jelenković and A. V. Phelps (unpublished); in *Proceedings of the Tenth International Conference on Gas Discharges and Their Applications, Swansea, Wales, 1992,* edited by W. T. Williams (University of Swansea, Swansea, Wales, 1992).

[14] H. Tisher and A. V. Phelps, Chem. Phys. Lett. **117**, 550 (1985); A. B. Wedding and A. V. Phelps, J. Chem. Phys. **89**, 2965 (1988).

[15] D. Levron and A. V. Phelps, J. Chem. Phys. **69**, 2260 (1978).

[16] A. V. Phelps (unpublished). Tabulations of several published dc voltage-current data sets for He, Ne, Ar, Kr, Xe, Hg, H$_2$, O$_2$, and N$_2$ are available in JILA Data Center Report No. 35 (1993) and on floppy disk.

[17] A. A. Kruithof and F. M. Penning, Physica **3**, 515 (1936).

[18] R. S. Sigmond, in *Proceedings of the Fourth International Conference on Ionization Phenomena in Ionized Gases, Uppsala, 1959,* edited by N. R. Nilsson (North-Holland, Amsterdam, 1960), Vol. 2, p. 189; in *Proceedings of the Fifth International Conference on Ionization Phenomena in Ionized Gases, Munich, 1961,* edited by H. Maecker (North-Holland, Amsterdam, 1962), p. 1359; in *Proceedings of the Ninth International Conference on Ionization Phenomena in Ionized Gases, Bucharest, 1969,* edited by G. Musa, I. Ghica, A. Popescu, and L. Năstase (Institute of Physics, Academy of Socialist Republic of Roumania, Bucharest, 1969), p. 129.

[19] F. Llewellyn-Jones, *Ionization and Breakdown in Gases* (Methuen, London, 1957), Fig. 4.5; A. L. Ward and E. Jones, Phys. Rev. **122**, 376 (1961).

[20] S. W. Downey, A. Mitchell, and R. A. Gottscho, J. Appl. Phys. **63**, 5280 (1988).

[21] H. Debontride, J. Derouard, P. Edel, R. Romestain, N. Sadeghi, and J.-P. Boeuf, Phys. Rev. A **40**, 5208 (1989).

[22] C. J. D. M. Verhagen, Physica **8**, 361 (1941).

[23] G. Ahsmann and H. J. Oskam, J. Appl. Phys. **29**, 1768 (1958).

[24] C. Yeh, J. Appl. Phys. **27**, 98 (1956).

[25] F. A. Benson, in *Proceedings of the Fifth International Conference on Ionization Phenomena in Ionized Gases, Munich, 1961* (Ref. [18]), p. 235.

[26] G. F. Weston, in *Proceedings of the Fifth International Conference on Ionization Phenomena in Ionized Gases, Munich, 1961* (Ref. [18]), p. 528.

[27] Chr. van Geel, Physica **6**, 806 (1939); Chr. van Geel, Appl. Sci. Res. **85**, 79 (1956).

[28] G. Ecker, W. Kröll, and O. Zöller, Ann. Phys. (Leipzig) **15**, 60 (1965).

[29] One of the authors (A.V.P.) has made extensive use of the review of theory in G. Ecker and K. G. Müller, Institüt für Theoretische Physik der Universität Bonn Technical Report No. FTR2 (1961) (unpublished), also presented as U. S. Army, European Research Office, Report No. DA-91-591-EUC-1254, 1961 (unpublished).

[30] K. G. Emeleus, Int. J. Electron. **42**, 105 (1977).

[31] See, for example, A. Garscadden, in *Gaseous Electronics, Electrical Discharges,* edited by M. N. Hirsh and H. J. Oskam (Academic, New York, 1978), Vol. I, p. 65.

[32] W. L. Nighan, in *Principles of Laser Plasmas,* edited by G. Bekefi (Wiley, New York, 1973), p. 272; R. Bruzzese, S. Solimeno, G. L. Braglia, and S. Martellucci, Nuovo Cimento **60B**, 113 (1980).

[33] The calculated capacitance of the electrodes is about 40 pF compared to the total circuit capacitance of 250 pF.

[34] D. A. Scott and A. V. Phelps, Phys. Rev. A **43**, 3043 (1991); **45**, 4198E (1992).

[35] A. Güntherschulze, Z. Phys. **49**, 358 (1928).

[36] B. N. Klyarfel'd, L. G. Guseva, and A. S. Pokrovskaya-Soboleva, Zh. Tekh. Fiz. **36**, 704 (1966) [Sov. Phys. Tech. Phys. **11**, 520 (1966)].

[37] See, for example, M. A. Townsend and W. A. Depp, Bell Syst. Tech. J. **32**, 1371 (1953); F. A. Benson and L. J. Bental, Wireless Engr. **32**, 330 (1955); Dj. A. Bošan, V. Ž. Zlatić, and B. J. Mijović, J. Phys. D **21**, 1462 (1988).

[38] B. M. Jelenković, Z. Lj. Petrović, and A. V. Phelps, Europhys. Conf. Abstr. **14E**, 22 (1990).